

Metallurgical and low-temperature electronic properties of $M_{1-x}U_xPd_3$ ($M=Sc, Y, La$) alloys

Donald A. Gajewski,* Ricky Chau, and M. Brian Maple

*Department of Physics and Institute for Pure and Applied Physical Sciences, University of California, San Diego,
La Jolla, California 92093*

(Received 5 May 1999)

In this paper, we compare the metallurgical and low-temperature electronic properties of the pseudo-binary alloy systems $Sc_{1-x}U_xPd_3$ and $Y_{1-x}U_xPd_3$ to gain insight into the nature of the non-Fermi-liquid (NFL) behavior observed in these systems at low temperatures. Our results show that both the $Sc_{1-x}U_xPd_3$ and $Y_{1-x}U_xPd_3$ systems exhibit similar NFL behavior, in spite of significant differences in their metallurgical properties. This comparison provides strong evidence that the NFL behavior is an intrinsic property, and not an extrinsic property driven by metallurgical disorder. Scanning electron microscopy and x-ray-diffraction measurements revealed that the U in the $Y_{1-x}U_xPd_3$ system is inhomogeneously distributed on the micron length scale, while the U in the $Sc_{1-x}U_xPd_3$ system is nearly homogeneously distributed. However, low-temperature measurements of the electronic specific heat coefficient $\gamma=C_p/T$, magnetic susceptibility χ , and electrical resistivity ρ show that the compounds $Sc_{0.7}U_{0.3}Pd_3$ and $Y_{0.8}U_{0.2}Pd_3$ exhibit the following NFL behavior with nearly the same Kondo temperature (T_K): $C_p/T \propto -(1/T_K)\ln(T/T_K)$, $\chi \propto 1 - (T/T_K)^{1/2}$, and $\rho \propto 1 - (T/T_K)$. We also report on the metallurgical properties of the related systems $La_{1-x}U_xPd_3$, $Y_{1-x}La_xPd_3$, and $La_{1-x}U_xPd_3$.

I. INTRODUCTION

A. Non-Fermi-liquid behavior

The $Y_{1-x}U_xPd_3$ pseudobinary alloy system has received considerable attention in the literature since the discovery of its unusual low-temperature electronic properties^{1,2} which are now collectively referred to as non-Fermi-liquid (NFL) behavior. However, there has been some debate about whether the so-called NFL behavior is an intrinsic electronic property or an extrinsic property associated with metallurgical inhomogeneity that several groups have reported is present in the bulk of their samples of $Y_{1-x}U_xPd_3$. We were thus motivated to study the metallurgical properties of our own samples of $M_{1-x}U_xPd_3$ ($M=Sc, Y, La, Th$) using scanning electron microscopy (SEM) and powder x-ray diffraction (XRD).

In this paper, we will show that while in the $Y_{1-x}U_xPd_3$ system the U is inhomogeneously distributed on a micron length scale, in the $Sc_{1-x}U_xPd_3$ system the U is nearly homogeneously distributed. However, in spite of this difference in their metallurgical properties, the $Y_{1-x}U_xPd_3$ and $Sc_{1-x}U_xPd_3$ systems display very similar NFL characteristics in their low-temperature physical properties and single-ion scaling with the U concentration and the Kondo temperature (T_K). These results suggest that the observed NFL behavior in these systems is intrinsic, and not a result of metallurgical inhomogeneity.

The NFL behavior in the $Y_{1-x}U_xPd_3$ system is manifested in electronic properties that diverge as a weak power law or logarithmic function of temperature at low temperature. Specifically, the electrical resistivity $\Delta\rho(T)$, the electronic specific heat coefficient $\gamma(T) \equiv \Delta C_p(T)/T$, and the intrinsic magnetic susceptibility $\Delta\chi(T)$ contributed by the U ions have the following form:

$$\Delta\rho(T)/\Delta\rho(0) \approx 1 - \alpha(T/T_K), \quad (1)$$

$$\gamma(T) \equiv \Delta C_p(T)/T \approx -(1/bT_K)\ln(T/T_K), \quad (2)$$

$$\Delta\chi(T)/\Delta\chi(0) \approx 1 - c(T/T_K)^{1/2}, \quad (3)$$

where α , b , and c are constants of order unity. These unusual temperature dependences occur over at least one decade of temperature for $T < T_K$. In contrast, the low-temperature electronic properties of a conventional Kondo system which behaves as a local Fermi liquid are

$$\Delta\rho(T)/\Delta\rho(0) \approx 1 - (T/T_K)^2, \quad (4)$$

$$\gamma(T) \equiv \Delta C_p(T)/T \approx \text{const}, \quad (5)$$

$$\Delta\chi(T)/\Delta\chi(0) \approx 1. \quad (6)$$

Since the discovery of this unusual NFL behavior in the $Y_{1-x}U_xPd_3$ system, similar temperature dependences of $\Delta\rho(T)$, $\Delta C_p(T)/T$, and $\Delta\chi(T)$ have also been observed in many other U- and Ce-based materials, including $UCu_{3.5}Pd_{1.5}$ (Ref. 3) and $CeCu_{5.9}Au_{0.1}$ (Ref. 4). These compounds have therefore been tentatively identified as a new class of f -electron materials whose physical properties exhibit what is now called NFL behavior at low temperature. The $Y_{1-x}U_xPd_3$ system is the first example of this class of materials (for reviews, see Refs. 5 and 6).

B. Summary of properties: Phase diagrams

First, we will briefly summarize some of the relevant physical properties of the $M_{1-x}U_xPd_3$ ($M=Sc, Y, La, Th$) systems. The phase diagram of the $Y_{1-x}U_xPd_3$ system is rich with interesting electronic and magnetic phenomena, as shown in Fig. 1(a). The $Y_{1-x}U_xPd_3$ system displays the Kondo effect for $x \leq 0.2$ and $T \geq T_K$. In this regime, the temperature dependence of the electrical resistivity is $\Delta\rho(T) \propto -\ln(T)$ and that of the magnetic susceptibility is $\Delta\chi(T)$

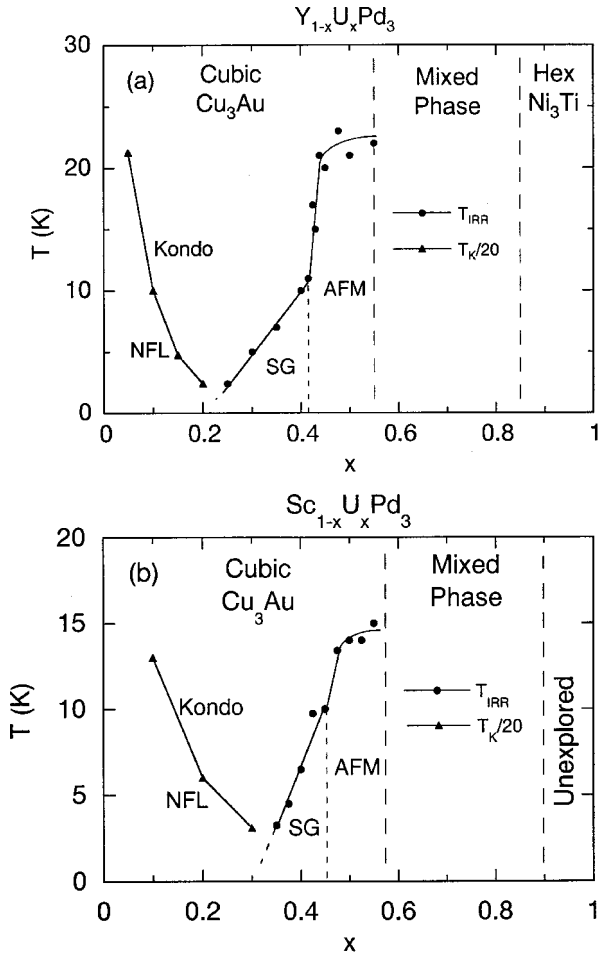


FIG. 1. Temperature T versus U concentration x phase diagram for (a) $Y_{1-x}U_xPd_3$ and (b) $Sc_{1-x}U_xPd_3$. NFL: non-Fermi liquid; SG: spin glass; AFM: antiferromagnet; T_{IRR} : irreversibility temperature (for magnetization); T_K : Kondo temperature.

$\propto(T + \Theta_{CW})^{-1}$, where Θ_{CW} is the Curie-Weiss temperature. The Kondo temperature T_K decreases exponentially with increasing x through a mechanism referred to as Fermi level tuning (FLT). In FLT, the substitution of U^{4+} for Y^{3+} results in an increase in the Fermi energy E_F and, in turn, an increase in the U $5f$ binding energy $\varepsilon_f = |E_F - E_{5f}|$. The Kondo temperature T_K varies exponentially with ε_f , and hence with x , through the relation

$$T_K \approx T_F \exp(-\varepsilon_f / [\langle V_{kf}^2 \rangle N(E_F)]), \quad (7)$$

where T_F is the Fermi temperature, $\langle V_{kf}^2 \rangle$ is the square of the conduction- $5f$ electron hybridization matrix element, and $N(E_F)$ is the density of states at E_F . The FLT picture was verified by photoemission spectroscopy (PES) and XRD experiments. The PES experiments revealed that E_F increases by ≈ 0.5 eV as x increases from 0 to 0.5 (Ref. 7). Subsequent PES experiments demonstrated that the core levels and valence band shift with E_F by comparing the $Y_{1-x}U_xPd_3$ spectra with the $Th_{1-x}U_xPd_3$ spectra.⁸ This increase in E_F is so large because the density of states at E_F of the host compound YPd_3 is relatively low. Seaman and Maple⁹ have confirmed that Sc, Y, and La are trivalent in $M_{1-x}U_xPd_3$, while

U and Th are tetravalent, through XRD measurements of the lattice parameters of $M_{1-x}U_xPd_3$ alloys with $M = Sc, Y, Pr$, and La.

Two types of magnetic ordering occur in the $Y_{1-x}U_xPd_3$ system for $0.25 \leq x \leq 0.55$: short-range spin glass (SG) ordering for $0.25 \leq x \leq 0.4$ and long-range antiferromagnetic ordering (AFM) for $0.41 \leq x \leq 0.55$, as shown in Fig. 1(a). The SG/AFM phase boundary has been established through electrical resistivity, magnetization, specific heat, and neutron diffraction measurements.^{10,11} In the SG regime, the magnetization is irreversible, with irreversibility temperatures T_{irr} that increase with increasing x , according to magnetization¹² and μ SR¹³ measurements. Neutron diffraction measurements by Dai *et al.*¹¹ revealed AFM ordering for the compound $Y_{0.55}U_{0.45}Pd_3$, with a Néel temperature T_N of 21 K and an ordered moment of $0.7\mu_B$ per U atom. The exact ordered magnetic structure can only be determined by neutron diffraction measurements on a suitable single crystal. However, Dai *et al.* have determined that the structure is composed of an antiferromagnetic stacking sequence in two directions with double the periodicity of the chemical unit cell, and a ferromagnetic stacking sequence in the third direction.

The $Sc_{1-x}U_xPd_3$ system exhibits the Kondo effect and low-temperature NFL properties similar to those of the $Y_{1-x}U_xPd_3$ system, as shown in the phase diagram in Fig. 1(b). However, in the $Sc_{1-x}U_xPd_3$ system, T_K has a higher value for a given x . In addition, the Kondo effect and NFL behavior are observed up to higher U concentrations ($x \leq 0.3$). This higher T_K is presumably brought about by the smaller ionic radius of Sc as compared to Y, which results in an increased $\langle V_{kf}^2 \rangle$, and, hence, a higher T_K . The $Sc_{1-x}U_xPd_3$ system also displays spin glass and AFM ordering similar to the $Y_{1-x}U_xPd_3$ system, but with $T_N \approx 14$ K in the AFM regime. The $La_{1-x}U_xPd_3$ system does not exhibit the Kondo effect, nor any non-Fermi-liquid-like temperature dependences in its physical properties.¹⁴ Therefore, the electronic properties of the $La_{1-x}U_xPd_3$ system will not be discussed further in this paper. However, we will discuss its structural properties, in relation to the $Sc_{1-x}U_xPd_3$ and $Y_{1-x}U_xPd_3$ systems.

II. EXPERIMENTAL DETAILS

Polycrystalline samples of $M_{1-x}X_xPd_3$ ($M = Sc, Y, \text{ or } La$; $X = U \text{ or } Th$) were prepared by arc-melting stoichiometric amounts of high purity (99.9% or better) elemental metals under an ultra-high purity (uhp) argon atmosphere. The elemental metals were carefully melted together as slowly as possible in order to minimize loss of some of the reactants caused by the reaction during the initial melt. The boule was melted for 5–15 sec, then allowed to cool to room temperature on the water-cooled copper hearth (which typically takes approximately 5 sec), and then turned over. This process was repeated 5 times in order to fully react all of the components. Less than 0.5% of the mass was lost during the melting process. Powder XRD measurements were performed on these samples with a Rigaku rotating-anode diffractometer using Cu $K\alpha$ radiation. Samples were prepared for SEM by polishing cross-sections of the boules with 1 micron or smaller diamond polishing compound. The SEM backscatter electron images were produced with the assistance of technicians at

the Scripps Institute of Oceanography Analytical Facility. Magnetic susceptibility measurements were made using a Quantum Design SQUID magnetometer from 1.8–300 K in applied fields up to 7 T, and a UCSD-built ^3He Faraday magnetometer from 0.4 K to 10 K in applied fields up to 6 T. Electrical resistivity measurements were made using a standard 4-wire ac technique at a frequency of 16 Hz. Specific heat $C_p(T)$ measurements were performed using a UCSD-built semiadiabatic heat pulse calorimeter from 0.5–20 K.

III. RESULTS

A. Powder x-ray diffraction (XRD)

The binary compounds MPd_3 ($M=Y, \text{Sc}$, and La) form in the cubic Cu_3Au structure, while the compounds XPd_3 ($X=U, \text{Th}$) form in the dhcp Ni_3Ti structure.¹⁵ Pseudobinary alloys of $M_{1-x}X_xPd_3$ form in the cubic Cu_3Au structure for $x \leq 0.55$ (with some exceptions, as will be discussed later), according to XRD measurements.^{9,14,16} Samples in the range $0.6 \leq x \leq 0.9$ are mixed phase, showing both cubic and hexagonal x-ray lines, while samples in the range $0.9 \leq x \leq 1$ form the Ni_3Ti structure.

The cubic lattice parameter (a) versus U concentration x for the $M_{1-x}U_xPd_3$ ($M=\text{Sc}, Y$) systems are shown in Fig. 2(a). These values agree reasonably well with other results published in the literature.^{2,9,17,18} As a result of the close match in ionic radius between Sc^{3+} , Y^{3+} and U^{4+} , the lattice parameter changes by less than 1% for $Y_{1-x}U_xPd_3$, and less than 2% for $\text{Sc}_{1-x}U_xPd_3$, across the phase diagram. However, the insensitivity of lattice parameter to U concentration makes difficult any attempt to detect nonrandom distributions of M and U in these samples (i.e., clustering) by measuring the breadth of the XRD peaks. The lattice parameter values extrapolate to that of theoretical cubic UPd_3 , which was deduced by Seaman and Maple via lattice parameter measurements of $M_{1-x}U_xPd_3$ ($M=\text{La}, \text{Pr}, Y, \text{Sc}$).⁹

Samples of $Y_{1-x}\text{Th}_xPd_3$ also form in the cubic Cu_3Au structure for $x \leq 0.55$ with a lattice parameter value that increases by approximately 2% across the phase diagram, as shown in Fig. 2(a). This is a larger change than in the $Y_{1-x}U_xPd_3$ system, since the ionic radius of Th^{4+} is greater than that of U^{4+} . Samples of $Y_{0.9-x}\text{Th}_xU_{0.1}Pd_3$ form in the cubic Cu_3Au structure only up to $x=0.4$. Thus, the solubility limit of total actinide elements ($X=U+\text{Th}$) in $Y_{1-x}X_xPd_3$ appears to be approximately $x=0.55$.

High resolution XRD measurements show that $\text{La}_{1-x}U_xPd_3$ also forms in the cubic Cu_3Au structure, but that the cubic XRD peaks are split, and can be fit to the sum of two peaks. These two peaks could represent the presence of two cubic phases in this sample with different lattice parameters, which we arbitrarily call phases ‘‘A’’ and ‘‘B.’’ Both lattice parameters of phases A and B generally decrease with increasing x , as shown in Fig. 2(b). This trend is in accordance with the U^{4+} ions having a smaller ionic radius than the La^{3+} ions. The intensity of the x-ray peaks provided an estimate of the relative volume fraction of phases A and B. For $x < 0.1$, the samples consist of approximately 90% phase A, while for $0.1 \leq x \leq 0.4$, the samples consist of comparable amounts of phases A and B. The ratio of phase B to phase A generally increases with increasing x . These results

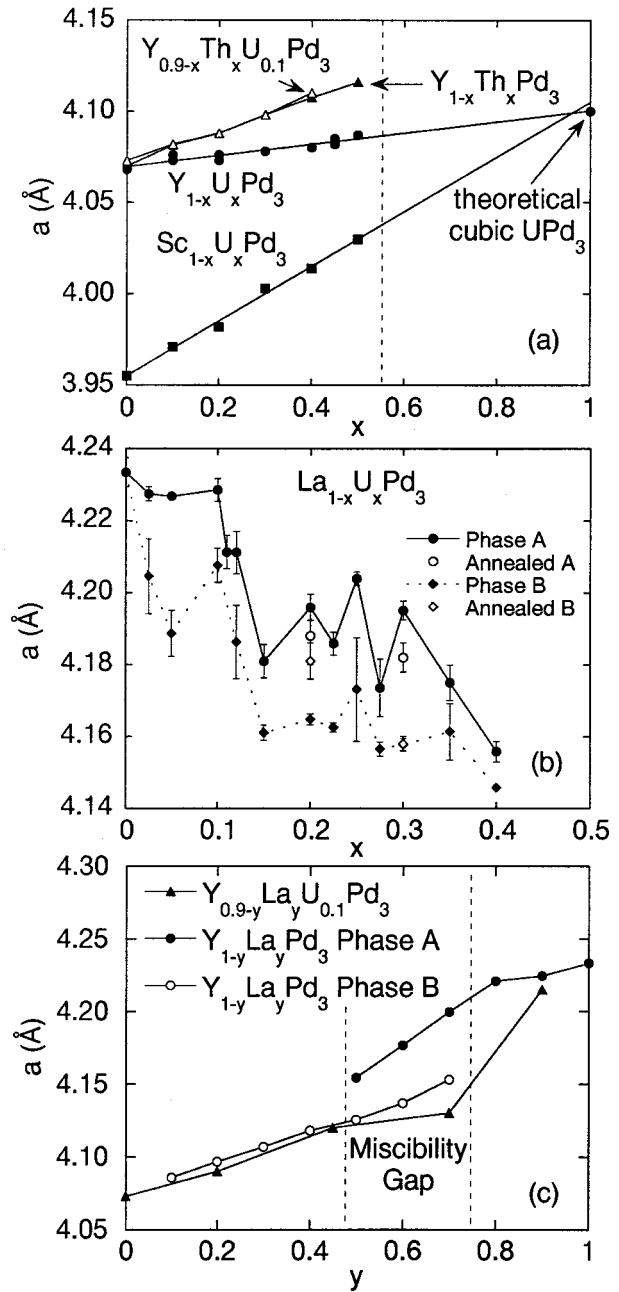


FIG. 2. (a) Cubic lattice parameter a versus U or Th concentration x for $M_{1-x}U_xPd_3$ ($M=\text{Sc}, Y$), $Y_{1-x}\text{Th}_xPd_3$, and $Y_{0.9-x}\text{Th}_xU_{0.1}Pd_3$ alloys. Solid lines are guides to the eye. See text for explanation of hypothetical cubic UPd_3 . (b) a versus U concentration x for phase A and phase B of $\text{La}_{1-x}U_xPd_3$. (c) a versus La concentration y for $Y_{0.9-y}\text{La}_yU_{0.1}Pd_3$, and phase A and phase B of $Y_{1-y}\text{La}_yPd_3$.

could indicate that the solubility limit of U in $\text{La}_{1-x}U_xPd_3$ is approximately $x=0.1$. Phase B could represent a cubic phase of $\text{La}_{1-x}U_xPd_3$ of a certain U concentration that forms preferentially.

In an attempt to obtain single phase samples of $\text{La}_{1-x}U_xPd_3$, two samples with $x=0.2$ and 0.3 , respectively, were sealed in a quartz tube under 0.2 atm of ultra high purity argon gas and annealed at 1200°C for one week. Subsequent XRD measurements showed that the samples still consisted of two cubic phases, but the lattice parameters of

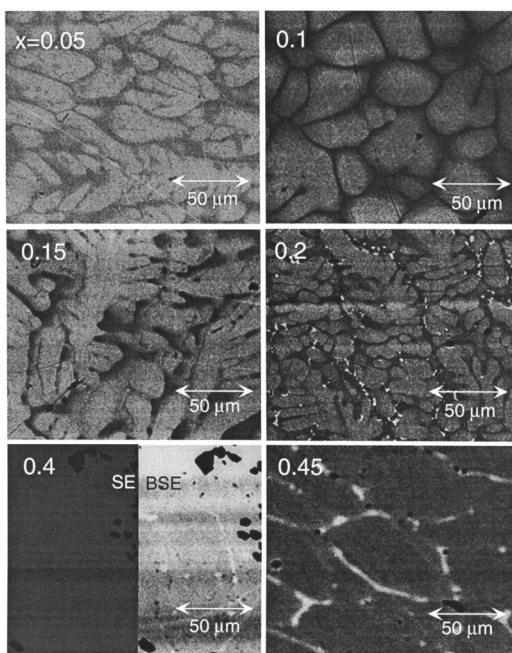


FIG. 3. BSE images of $Y_{1-x}U_xPd_3$ alloys. For $x=0.4$, left: SEC; right: BSE.

the two cubic phases were closer to each other than for unannealed samples. This result suggests that annealing at high enough temperatures for a sufficiently long time could yield a single phase sample. However, such annealing could risk extensive loss of palladium in these alloys, as was suggested by Süllow *et al.*¹⁹

Plots of the cubic lattice parameter versus lanthanum concentration (y) for the $Y_{0.9-y}La_yU_{0.1}Pd_3$ and $Y_{1-y}La_yPd_3$ systems are shown in Fig. 2(c). The samples of $Y_{1-y}La_yPd_3$ are single phase for $0 \leq y \leq 0.4$ and $0.8 \leq y \leq 1$. However, a miscibility gap occurs for $0.5 \leq x \leq 0.7$, in which the XRD peaks are split in a similar fashion as in the $La_{1-x}U_xPd_3$ system. Outside of this miscibility gap, the lattice parameters of $Y_{0.9-y}La_yU_{0.1}Pd_3$ and $Y_{1-y}La_yPd_3$ agree reasonably well, but inside of the miscibility gap, these lattice parameters do not agree well. This result indicates that samples of $Y_{0.9-y}La_yU_{0.1}Pd_3$ and $Y_{1-y}La_yPd_3$ with $0.5 \leq y \leq 0.7$ contain gross inhomogeneities.

B. Scanning electron microscopy (SEM)

The intensity of backscattered electron (BSE) images taken with an SEM is proportional to the local atomic number of the sample. Therefore, these BSE images yield semi-quantitative information about composition homogeneity in a sample. In BSE images of samples of $M_{1-x}U_xPd_3$, regions of higher intensity correspond to U-rich $M_{1-x}U_xPd_3$ (i.e., $x_{\text{actual}} > x_{\text{nominal}}$), while darker regions correspond to M-rich $M_{1-x}U_xPd_3$ (i.e., $x_{\text{actual}} < x_{\text{nominal}}$). We assume that Pd is uniformly distributed in these samples of $M_{1-x}U_xPd_3$, based on the results of other groups and the fact that XRD measurements did not reveal the presence of crystalline impurities such as elemental metals or UPd_3 . We used secondary electron (SE) images to distinguish composition fluctuations from physical voids in the sample. Unfortunately, we could not perform a quantitative electron probe microanalysis

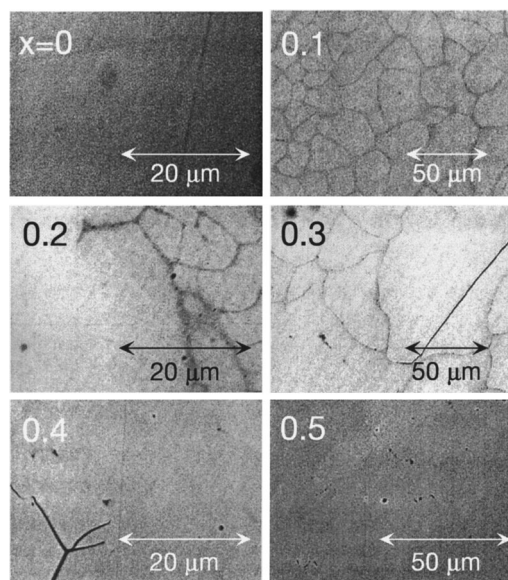


FIG. 4. BSE images of $Sc_{1-x}U_xPd_3$ alloys.

(EPMA) at this time because the SEM we used can only access an energy range in which the spectral lines of U and Pd overlap.

The BSE images of samples of $Y_{1-x}U_xPd_3$ with $0.05 \leq x \leq 0.2$ reveal a significant fraction of micron-sized Y-rich and U-rich regions throughout their cross-sections, as shown in Fig. 3. The majority volume fraction of samples of $Y_{1-x}U_xPd_3$ consist of dendrite-like grains of approximately uniform U concentration, separated by darker Y-rich intergranular regions. The sample of $Y_{0.8}U_{0.2}Pd_3$ appears to contain the most severe phase separation, with some small U-rich regions (white spots) in addition to the dendritic Y-rich regions. Samples with $x=0.4$ and 0.45 are much more homogeneous than those with lower composition, with over 98% of the sample of a single phase as estimated from the SEM images. Black spots that appear in split screen images (BSE and SE) are most likely physical voids in the samples. BSE images of the undoped compound YPd_3 indicate that the sample is homogeneous throughout. These images are typical of cross sections of approximately (0.5–3) gram arc-melted samples, taken near the middle of the samples. However, BSE images taken near the bottom of the samples (closer to the water-cooled copper hearth) generally reveal a smaller volume fraction of off-stoichiometry material relative to the bulk. Since the bottom of the sample solidifies more quickly, this suggests that single phase samples might be obtained if the samples could be cooled quickly enough from the melt. We also observed that while samples with $x=0.2$ or less are very brittle, samples with $x \geq 0.4$ tend to be less brittle. This observation suggests that samples of $Y_{1-x}U_xPd_3$ near $x=0.45$ are metallurgically more stable.

These results are qualitatively similar to those of other groups. EPMA measurements by Süllow *et al.* indicate variations in x as high as 30% of the nominal x on the scale of $10 \mu\text{m}$.¹⁹ Süllow *et al.* speculated that the phase diagram of this pseudobinary alloy exhibits a solidus line and a liquidus line, similar to that seen in binary alloys. Such a condition would cause the precipitation of off-stoichiometric regions in the sample upon cooling from the liquid phase, as governed

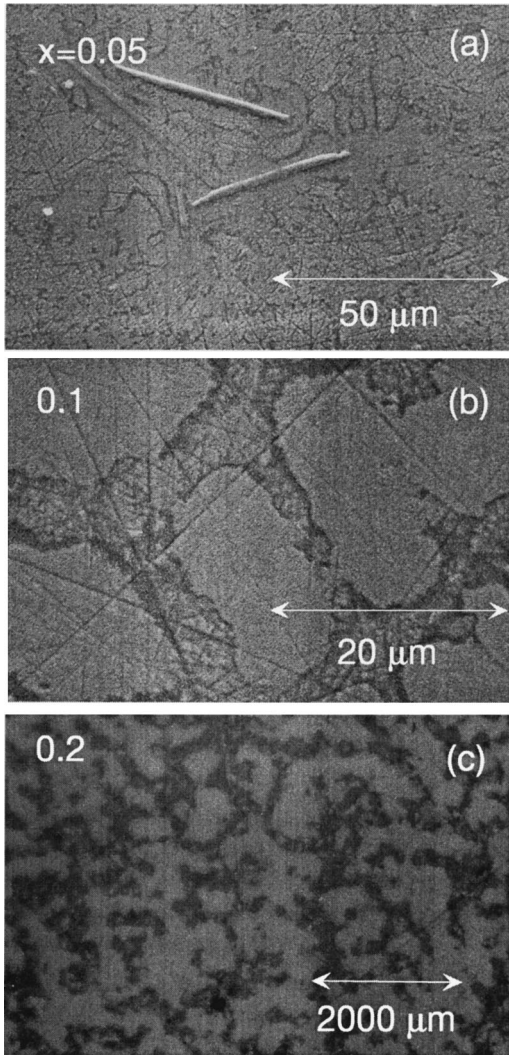


FIG. 5. (a) BSE image of $\text{La}_{0.95}\text{U}_{0.05}\text{Pd}_3$. (b) BSE image of $\text{La}_{0.9}\text{U}_{0.1}\text{Pd}_3$. (c) Optical image of $\text{La}_{0.8}\text{U}_{0.2}\text{Pd}_3$.

by the lever rule. This could explain the variations in x observed in the SEM studies. Süllow *et al.* also found that annealing at temperatures as high as 1500°C reduced, but did not eliminate, the inhomogeneities. They speculated that higher temperature or longer time annealing could homogenize the samples. However, such annealing could increase the amount of Pd loss. The results of Xu *et al.*²⁰ indicate even larger variations in x than those observed by Süllow *et al.* Xu *et al.* found that these concentration fluctuations persist in smaller (≈ 0.2 g) arc-melted ingots, even though one might expect that smaller samples would cool faster from the melt into the solid form, and, hence, to more homogeneous samples.

Preliminary measurements of the diffuse scattering of synchrotron x rays on a sample of $\text{Y}_{0.8}\text{U}_{0.2}\text{Pd}_3$ have been performed by J.L. Robertson *et al.*²¹ The diffuse scattering data were modeled to estimate the non-random distribution of Y and U in this sample. The diffuse scattering data were fitted using three different models: random Y/U distribution, 5% clustering of Y/U, and an ordered arrangement of Y/U. Robertson *et al.* found that the 5% clustering model provided the best fit to the data and concluded that there is less than 1% occupation of the Pd sites by U. Thus, these preliminary

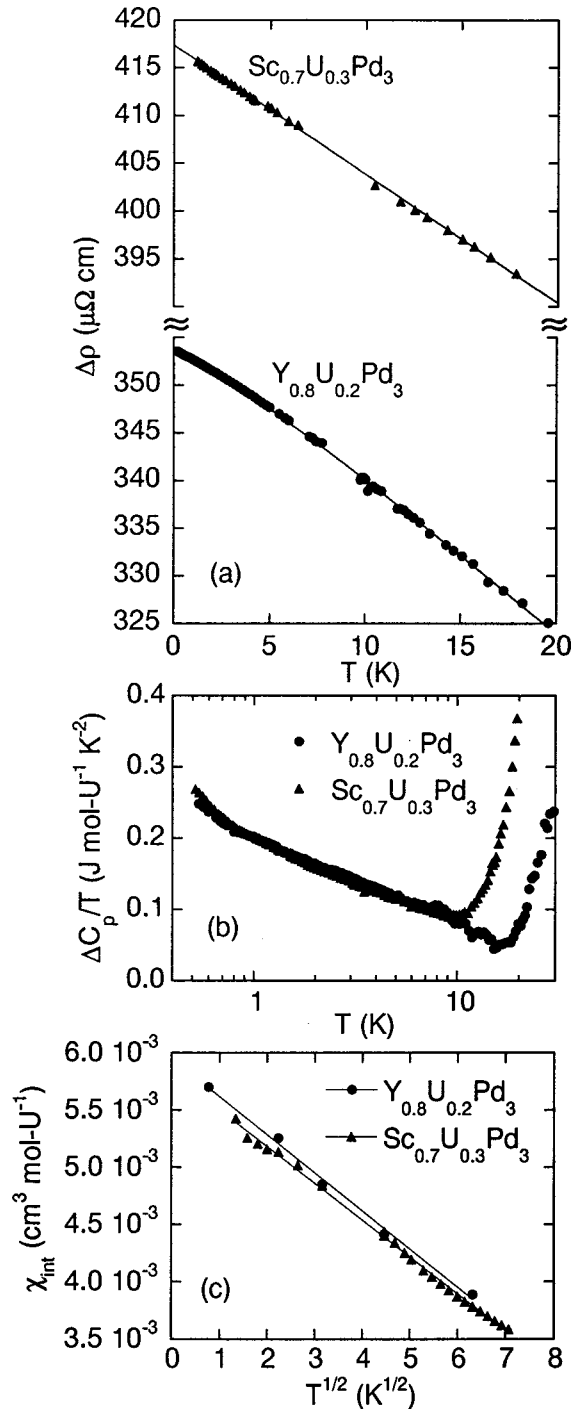


FIG. 6. (a) U contribution to the electrical resistivity $\Delta\rho$ versus T of $\text{Sc}_{0.7}\text{U}_{0.3}\text{Pd}_3$ and $\text{Y}_{0.8}\text{U}_{0.2}\text{Pd}_3$. Solid lines are fits as described in the text. (b) U contribution to the electronic specific heat coefficient $\Delta C_p/T$ versus T on a semilogarithmic scale. (c) Intrinsic magnetic susceptibility χ_{int} versus $T^{1/2}$. Solid lines are fits as described in the text.

results indicate that on the 50 \AA scale, the U concentration fluctuations are no more than $\approx 10\%$ of the nominal U composition.

Figure 4 shows SEM images of samples of $\text{Sc}_{1-x}\text{U}_x\text{Pd}_3$ with $0 \leq x \leq 0.5$. The sample of ScPd_3 is homogeneous in all regions that were scanned. Samples with $0.1 \leq x \leq 0.3$ appear to consist almost completely of large grains of apparently single phase material, separated by a small amount ($< 1\%$

by volume) of intergranular material. These small regions are not physical voids, as determined by comparing the BSE and SE images, but likely consist of $\text{Sc}_{1-x}\text{U}_x\text{Pd}_3$ with slightly lower U concentration than the bulk. Samples of $\text{Sc}_{1-x}\text{U}_x\text{Pd}_3$ with $0.4 \leq x \leq 0.5$ appear to be completely homogeneous. The small black spots and lines, however, are voids in the samples. These inhomogeneities in $\text{Sc}_{1-x}\text{U}_x\text{Pd}_3$ comprise a much smaller volume fraction than in $\text{Y}_{1-x}\text{U}_x\text{Pd}_3$. In addition, samples of $\text{Sc}_{1-x}\text{U}_x\text{Pd}_3$ seem to be much less brittle than samples of $\text{Y}_{1-x}\text{U}_x\text{Pd}_3$. Therefore, the metallurgical properties of $\text{Sc}_{1-x}\text{U}_x\text{Pd}_3$ appear to be superior to those of $\text{Y}_{1-x}\text{U}_x\text{Pd}_3$.

The BSE images of $\text{La}_{1-x}\text{U}_x\text{Pd}_3$ shown in Fig. 5 reveal the presence of gross inhomogeneities. Energy dispersive x-ray measurements revealed that the rodlike inclusions shown in the image of $\text{La}_{0.95}\text{U}_{0.05}\text{Pd}_3$ consist of elemental lanthanum. Inhomogeneities in a sample of $\text{La}_{0.8}\text{U}_{0.2}\text{Pd}_3$ are even visible in an optical photograph; however, the exact compositions of the various regions in the sample have not yet been determined. These inhomogeneities are consistent with the double x-ray-diffraction peaks discussed earlier and could be a result of the large mismatch in ionic radius between La and U ions in this compound.

C. Low-temperature electronic properties

As shown in Fig. 6, the low-temperature NFL electronic properties of the compounds $\text{Y}_{0.8}\text{U}_{0.2}\text{Pd}_3$ and $\text{Sc}_{0.7}\text{U}_{0.3}\text{Pd}_3$ scale with nearly the same Kondo temperature T_K . This nearly identical scaling can be understood through FLT. The conduction electron density of $\text{Sc}_{0.7}\text{U}_{0.3}\text{Pd}_3$ is higher than that of $\text{Y}_{0.8}\text{U}_{0.2}\text{Pd}_3$, which would yield a smaller value of T_K for $\text{Sc}_{0.7}\text{U}_{0.3}\text{Pd}_3$. However, the lattice parameter value of $\text{Sc}_{0.7}\text{U}_{0.3}\text{Pd}_3$ is lower than that of $\text{Y}_{0.8}\text{U}_{0.2}\text{Pd}_3$, which would yield a larger value of T_K for $\text{Sc}_{0.7}\text{U}_{0.3}\text{Pd}_3$. Thus, these two effects approximately balance each other, resulting in nearly identical T_K values for $\text{Y}_{0.8}\text{U}_{0.2}\text{Pd}_3$ and $\text{Sc}_{0.7}\text{U}_{0.3}\text{Pd}_3$.

The U contributions to the electrical resistivity $\Delta\rho(T)$ of the compounds $\text{Y}_{0.8}\text{U}_{0.2}\text{Pd}_3$ and $\text{Sc}_{0.7}\text{U}_{0.3}\text{Pd}_3$ increase approximately linearly with decreasing temperature down to the lowest measured temperature. The solid lines are least squares fits to the functional form $\Delta\rho(T) = \Delta\rho(0)(1 - \alpha(T/T_K)^n)$, where $\Delta\rho(0)$, T_K , and n are all equivalent adjustable fitting parameters. For $\text{Y}_{0.8}\text{U}_{0.2}\text{Pd}_3$, $n = 1.1$ and $T_K = 49$ K, while for $\text{Sc}_{0.7}\text{U}_{0.3}\text{Pd}_3$, $n = 1.0$ and $T_K = 72$ K. The value of the phenomenological parameter $\alpha = 0.23$ was chosen so that the value of T_K extracted from the low-temperature fit roughly agrees with the value extracted from the high-temperature fit, as described in Ref. 22. The quantity $\Delta\rho(T)$ was obtained by subtracting $\rho(T)$ of the host, YPd_3 or ScPd_3 , respectively, from the measured $\rho(T)$.

The U contributions to the electronic specific heat coefficient $\Delta C_p(T)/T$ of the compounds $\text{Y}_{0.8}\text{U}_{0.2}\text{Pd}_3$ and $\text{Sc}_{0.7}\text{U}_{0.3}\text{Pd}_3$ diverge logarithmically with decreasing tem-

perature over more than one decade in temperature, as plotted in Fig. 6(b). The quantity $\Delta C_p(T)$ was determined by subtracting an estimated phonon term βT^3 from the measured $C_p(T)$. The value of β was obtained by scaling the literature values of β for ScPd_3 and YPd_3 (Ref. 23) by the molecular weights of $\text{Sc}_{0.7}\text{U}_{0.3}\text{Pd}_3$ and $\text{Y}_{0.8}\text{U}_{0.2}\text{Pd}_3$, respectively. The upturns in $\Delta C_p(T)/T$ at higher temperatures are likely due to either an incorrect subtraction of the phonon specific heat or a Schottky anomaly associated with crystalline electric field levels. A fit of the $\Delta C_p(T)/T$ data to the two-channel spin- $\frac{1}{2}$ Kondo model yields a value of T_K of ≈ 40 K for both $\text{Sc}_{0.7}\text{U}_{0.3}\text{Pd}_3$ and $\text{Y}_{0.8}\text{U}_{0.2}\text{Pd}_3$.^{1,24}

The intrinsic magnetic susceptibilities $\chi_{\text{int}}(T)$, shown in Fig. 6(c), for these compounds are also nearly identical, saturating to a constant as $T^{1/2}$ with decreasing temperature. The intrinsic susceptibility $\chi_{\text{int}}(T)$ was obtained by subtracting an estimated extrinsic impurity contribution, as described in Ref. 22. The solid lines are least squares fits to the functional form $\chi_{\text{int}}(T) = \chi(0)\{1 - c(T/T_K)^{1/2}\}$. The quantities $\chi(0)$ and T_K are equivalent adjustable fitting parameters, while c is a phenomenological parameter, whose value is 0.36, which is similar to the parameter α in expression (1) for the resistivity, as described above. The fits yield nearly identical values of T_K and $\chi(0)$ for these compounds. For $\text{Y}_{0.8}\text{U}_{0.2}\text{Pd}_3$, $\chi(0) = 5.9 \times 10^{-3} \text{ cm}^3 \text{ mol U}^{-1}$ and $T_K = 42$ K. For $\text{Sc}_{0.7}\text{U}_{0.3}\text{Pd}_3$, $\chi(0) = 5.8 \times 10^{-3} \text{ cm}^3 \text{ mol U}^{-1}$ and $T_K = 43$ K.

IV. CONCLUSIONS

The similarity of the physical properties of the compounds $\text{Sc}_{0.7}\text{U}_{0.3}\text{Pd}_3$ and $\text{Y}_{0.8}\text{U}_{0.2}\text{Pd}_3$ is striking in view of their qualitatively different metallurgical microstructure. In addition, the $\text{Sc}_{1-x}\text{U}_x\text{Pd}_3$ and $\text{Y}_{1-x}\text{U}_x\text{Pd}_3$ systems display very similar low-temperature single-ion scaling and NFL behavior, even though U concentration fluctuations appear to be more significant in $\text{Y}_{1-x}\text{U}_x\text{Pd}_3$. These results suggest that the observed NFL behavior in the $\text{Y}_{1-x}\text{U}_x\text{Pd}_3$ system is dominated by the majority uniform matrix in the materials, and not by the smaller Y-rich and U-rich regions observed in the SEM images. However, the results of the metallurgical study of the alloy systems described herein do not rule out a significant role of intrinsic disorder in the physics underlying the observed NFL behavior in these compounds.

ACKNOWLEDGMENTS

This research was supported by the National Science Foundation under Grant No. DMR-97-05454. We thank James F. Smith and John Neumeier of Los Alamos National Laboratory for performing several preliminary scanning electron microscopy measurements and informative discussions. We also thank Donald Swenholt, Marcio de Andrade, and Andreas Amann for assistance in refining the manuscript.

*Present address: NIST, Bldg. 225, Rm. A-365, Gaithersburg, MD 20899.

¹C.L. Seaman, M.B. Maple, B.W. Lee, S. Ghamaty, M.S. Torikachvili, J.S. Kang, L.Z. Liu, J.W. Allen, and D.L. Cox, Phys. Rev. Lett. **67**, 2882 (1991).

²B. Andraka and A.M. Tsvetlik, Phys. Rev. Lett. **67**, 2886 (1991).

³B. Andraka and G.R. Stewart, Phys. Rev. B **47**, 3208 (1993).

⁴H. von Lohneysen, T. Pietrus, G. Portisch, H.G. Schlager, A. Schroder, M. Sieck, and T. Trappmann, Phys. Rev. Lett. **72**, 3262 (1994).

- ⁵M.B. Maple, M.C. de Andrade, J. Herrmann, Y. Dalichaouch, D.A. Gajewski, C.L. Seaman, R. Chau, R. Movshovich, M.C. Aronson, and R. Osborn, *J. Low Temp. Phys.* **99**, 223 (1994).
- ⁶M.B. Maple, M.C. de Andrade, J. Herrmann, S.H. Han, R. Movshovich, D.A. Gajewski, and R. Chau, *Physica C* **263**, 490 (1995).
- ⁷J.S. Kang, J.W. Allen, M.B. Maple, M.S. Torikachvili, W.P. Ellis, B.B. Pate, Z.X. Shen, J.J. Yeh, and I. Lindau, *Phys. Rev. B* **39**, 13 529 (1989).
- ⁸J.W. Allen, L.Z. Liu, R.O. Anderson, C.L. Seaman, M.B. Maple, Y. Dalichaouch, J.S. Kang, and M.S. Torikachvili, *Physica B* **188**, 307 (1993).
- ⁹C.L. Seaman and M.B. Maple, *Physica B* **199**, 396 (1993).
- ¹⁰D.A. Gajewski, N.R. Dilley, R. Chau, and M.B. Maple, *J. Phys.: Condens. Matter* **8**, 9793 (1996).
- ¹¹P. Dai, H.A. Mook, C.L. Seaman, M.B. Maple, and J.P. Koster, *Phys. Rev. Lett.* **75**, 1202 (1995).
- ¹²C.L. Seaman, M.B. Maple, B.W. Lee, S. Ghamaty, M.S. Torikachvili, J.S. Kang, L.Z. Liu, J.W. Allen, and D.L. Cox, *J. Alloys Compd.* **181**, 327 (1991).
- ¹³W.D. Wu, A. Keren, L.P. Le, G.M. Luke, B.J. Sternlieb, Y.J. Uemura, C.L. Seaman, Y. Dalichaouch, and M.B. Maple, *Phys. Rev. Lett.* **72**, 3722 (1994).
- ¹⁴M.B. Maple, D.A. Gajewski, R. Chau, P. Dai, H.A. Mook, R. Movshovich, and C.L. Seaman, *Physica B* **223**, 447 (1995).
- ¹⁵R.P. Elliot, *Constitution of Binary Alloys*, First Supplement (McGraw-Hill, New York, 1965).
- ¹⁶C.L. Seaman, Ph.D. dissertation, University of California, San Diego, 1991.
- ¹⁷Y. Aoki, K. Terayama, H. Sato, K. Maeda, and Y. Onuki, *Physica B* **206**, 451 (1994).
- ¹⁸C. Koenig, *Z. Phys. B: Condens. Matter* **50**, 33 (1983).
- ¹⁹S. Süllo, T.J. Gortenmulder, G.J. Nieuwenhuys, A.A. Menovskiy, and J.A. Mydosh, *J. Alloys Compd.* **215**, 223 (1994).
- ²⁰J. Xu, P.J.C. Signore, B. Andraka, W.A. Acree, M.W. Meisel, and Y. Takano, *J. Alloys Compd.* **216**, 33 (1994).
- ²¹J.L. Robertson, P. Dai, D.A. Gajewski, and M.B. Maple (unpublished).
- ²²M.B. Maple, C.L. Seaman, D.A. Gajewski, Y. Dalichaouch, V.B. Barbeta, M.C. de Andrade, H.A. Mook, H.G. Lukefahr, O.O. Bernal, and D.E. MacLaughlin, *J. Low Temp. Phys.* **95**, 225 (1993).
- ²³M.J. Besnus, J.P. Kappler, and A. Meyer, *J. Phys. F: Met. Phys.* **13**, 597 (1983).
- ²⁴D.A. Gajewski, P. Allenspach, C.L. Seaman, and M.B. Maple, *Physica B* **199**, 419 (1993).